SYNTACTIC AND COMPOSITE FOAMS

Designing compressive properties of titanium foams

Nihan Tuncer · Gursoy Arslan

Abstract Titanium foams were produced by optimizing a relatively cheap method, sintering under flowing high purity argon gas with fugitive space holder. Removal of the space holder was conducted by dissolution in hot deionized water which renders it possible to minimize contamination of titanium. Titanium foams having various densities between 20 and 70% were manufactured and systematically characterized. Pore sizes varying from a few microns up to 2 mm were obtained. Compatibility with well known porosity–mechanical property formulations of cellular solids was investigated. Pore sizes in the investigated range were found to have a negligible effect on the elastic portion of compressive stress–strain diagram. High strain rate tests revealed that increasing the strain rate increases compressive strength of the titanium foams produced. The onset strain of densification of the produced titanium foams was determined by the recently developed energy absorption efficiency method. The energy absorbed per unit volume was then calculated by referring to the pre-determined onset strain of densification. A plot of energy absorbed per unit volume (E_A) as a function of relative density (ρ/ρ_s) at various strains (%ε) suggested that the data could be fitted to an equation of the form $E_A = A(\%\varepsilon)^B(\rho/\rho_s)^C$, where A, B and C are constants, for both fine- and coarse-pored titanium foams.

N. Tuncer (✉) · G. Arslan
Department of Materials Science and Engineering, Faculty of Engineering and Architecture, Anadolu University, Iki Eylul Campus, 26480 Eskisehir, Turkey
e-mail: nihant@anadolu.edu.tr

Introduction

Among metal foams, titanium (Ti) foams are preferred in many crucial applications in which aggressive media are involved, high temperatures occur or biocompatibility is required [1, 2]. Since most of the applications, especially biomedical and energy absorbing ones, include compressive load bearing, manufacturing of foam structures necessitates a well comprehension of the compression behaviour. However, there are only a few numbers of systematic studies on the compressive behaviour of Ti foams, most of which are limited to relatively narrow porosity ranges [3]. Since mechanical properties strongly depend on the production method and resulting microstructure, manufacturing of Ti foams that is well-responding to design requirements necessitates a detailed analysis on the effects of microstructure and strain rates.

Cellular metals generally have a good energy absorbing capability because of their unique extensive plateau regime [1, 2]. Ti foams have potential applications in areas such as car crash protection, shipbuilding in luxury boats, automotive industry and armour for which energy absorption properties are of importance [4]. Although energy absorption and pore structure relation has been studied extensively for aluminium and steel foams [5, 6], there has not yet been a systematic approach to characterize the energy absorption behaviour of Ti foams.

In this study, Ti foams having different levels of porosity were produced by space holder method and compressively tested in order to obtain a relationship between pore characteristics and compressive behaviour. For removal of space holder, which constitutes a threat for contamination of Ti, water dissolution method was preferred [7]. This method provides an easier foaming step ending up with a possibly cleaner environment for sintering

and thus a reduced risk of contamination. Furthermore, this method shortens the removal time from dozens of hours to just a few hours. No negative effect of the dissolution removal on mechanical properties was observed. Produced foams were characterized by considering the relationship between the pore structure and compressive properties.

Experimental

Ti foams were manufactured by space holder method using Grade 2 commercially pure (cp) Ti powder, supplied by Alfa Aesar, Germany, with an average particle size (d_{50}) of 23.5 μm, as measured with a Mastersizer 2000 particle size analyser. Angular-shaped Ti powders (Fig. 1) were preferred in order to increase the packing efficiency without using a binder, since preforms pressed from spherical powders tend to collapse during removal of the space holder. The particle size range of the coarse and fine carbamide ($CO(NH_2)_2$) space holder varied between 0.5–2 mm and 0.1–0.5 mm, respectively (Fig. 2).

Space holder and Ti powders were dry mixed in a ZrO_2 medium using ball milling for 18 h. The mixtures, prepared in different proportions, were first pressed at 150 MPa uniaxially in steel dies to ease handling. The preforms were then cold isostatically pressed at 300 MPa in order to prevent collapse of the green body during space holder removal.

Carbamide was leached out completely, as confirmed by weighing the specimens before and after the space holder removal step, in hot deionized water without destroying the green skeleton (Fig. 3) which then were sintered in a tubular furnace at 1200 °C for 2 h under flowing argon (Ar) gas after being vacuumed and purged with Ar gas three times. The high purity Ar gas contained 1 ppm
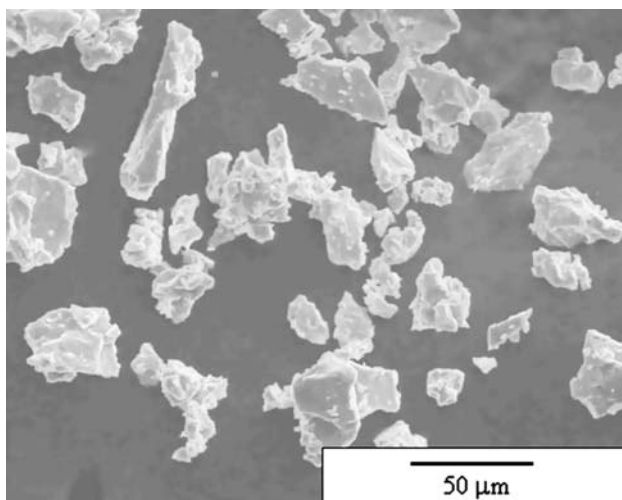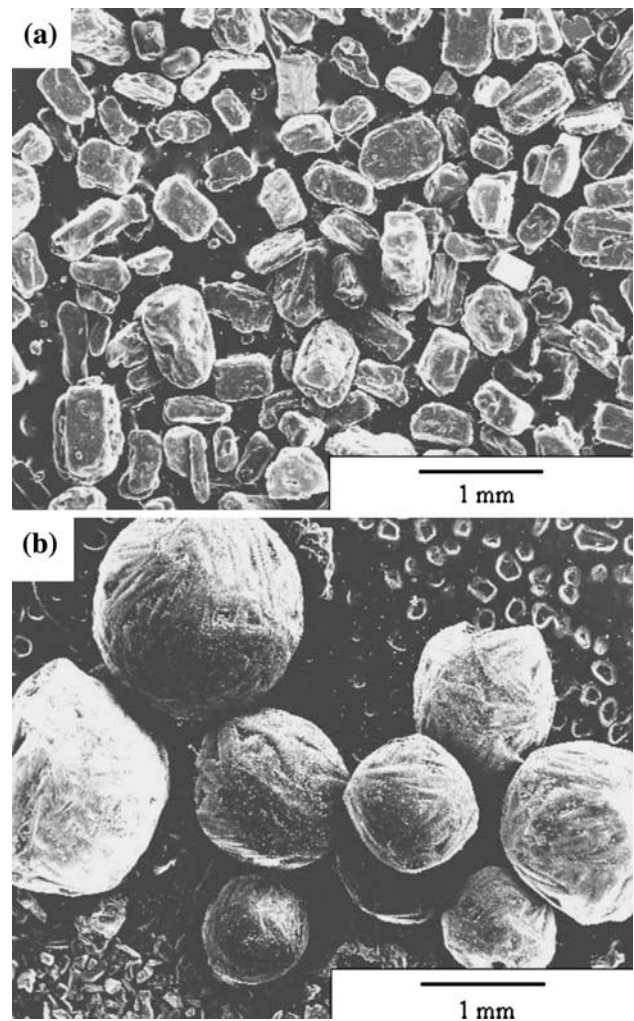

Fig. 1 Angular-shaped Ti powders used in this study

Fig. 2 SEM images of space holder powders used in this study. **a** coarse and **b** fine carbamide

oxygen, 3.1 ppm nitrogen and 2 ppm hydrogen, as given by the supplier. The resulting sintered Ti foam blocks were cut into nine pieces and the bulk densities were measured separately in order to confirm reproducibility.

Microstructures of the foams were analysed with a scanning electron microscope (SEM, Zeiss Supra 50 VP).

O, N and H content measurements were performed with a LECO TCH 600 Simultaneous O, N, H Determinatior.

Compression tests with quasistatic (10^{-3} s^{-1}) and medium (10^{-1} s^{-1}) strain-rates were conducted on samples having cross-sectional areas of around 55 mm^2 and length-to-width ratios of about 1.8. Compression tests were carried out at room temperature with an Instron 5581 model Mechanical Testing Machine. Strains were calculated from the cross-sectional displacement of the crosshead. The axis of compression was parallel to the compaction direction. Compression cages were lubricated in order to minimize friction between the sample and the cages. Compression
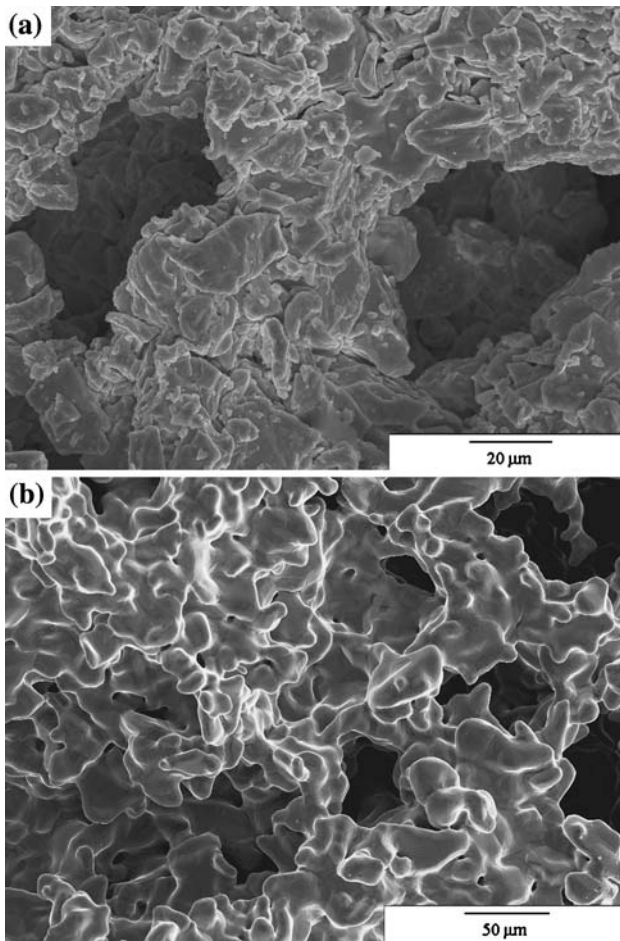
Fig. 3 SEM micrographs of the foams after **a** carbamide removal and **b** sintering

Table 1 O, N and H content in starting Ti powder and produced foams

	Alfa Aesar Ti powder	Ti foams produced
O (wt%)	0.230	0.395
N (wt%)	0.017	0.060
H (ppm)	0.022	0.048

strengths were determined by using 0.2% offset method. High strain rate compression tests were performed using a compression type Split Hopkinson Pressure Bar (SHBP) set-up with aluminium bars. An average maximum strain rate of $600 \ \text{s}^{-1}$ was applied to all of the specimens.

Results and discussion

Effect of pore size and content on mechanical properties

The scatter in the bulk densities of nine specimens from the same block was below 0.8% which implies a homogeneous distribution of porosity in the foams fabricated from fine carbamide powder. The density scatter, approximately 3%, was higher for coarse-pored foams since homogeneous mixing is not possible due to the large difference in particle size and density of Ti and carbamide powders.

Due to the extreme affinity of Ti to atmospheric gases like O, N and H, and their presence in ppm level in the furnace atmosphere, an increase in the concentration of these elements was observed after sintering (Table 1), which makes the wall material of the foams behave like Grade 4 Ti rather than Grade 2 Ti. Since the interstitial content is a critical strengthening factor in Ti, the compressive strength (650 MPa) and elastic modulus (110 GPa) values of Grade 4 Ti, given in ASTM standard F67-89 [8], were referred to in the calculations although Grade 2 Ti powder was used.

Mercury porosimeter measurements showed that the use of fine carbamide powder resulted in a monomodal pore size distribution between 5 and 200 μm with a peak point at 75 μm. Incorporation of large (>50 vol.%) amounts of fine carbamide powder promoted pore coalescence resulting in pores having diameters of up to 400 μm. Coarse carbamide powders, on the other hand, resulted in a bimodal distribution with a large pore size difference. Primary pores (Fig. 4a) formed by carbamide powder and secondary pores within the cell walls (Fig. 4b, c) had size ranges varying between 0.5–2 mm and 5–25 μm, respectively, resulting in Ti foams having an interconnected pore structure. This fact enables the use of mechanical property formulations suggested for open-pore foams [1].

Compression tests of cellular Ti materials having porosities in the range of 20–70% showed that the compressive strength decreases and the plateau region increases smoothly with increasing porosity content (Fig. 5). As relative density increases the plateau region becomes more ambiguous. The smooth character of the curves confirms the ductile behaviour of the foams in the porosity range studied.

The data of relative compressive strength of the fine- (75 μm) and coarse- (up to 2 mm) pored foams produced as a function of relative density were fitted to the empirical equations suggested by Gibson and Ashby [1] in which a fixed density exponent of 1.5 is pre-assumed:

$$\frac{\sigma_{ys}^*}{\sigma_{ys}} = 1.05 \cdot \left(\frac{\rho^*}{\rho_s}\right)^{1.5} - 0.16 \quad \text{(fine-pored)} \qquad (1a)$$

$$\frac{\sigma_{ys}^*}{\sigma_{ys}} = 1.02 \cdot \left(\frac{\rho^*}{\rho_s}\right)^{1.5} - 0.15 \quad \text{(coarse-pored)} \qquad (1b)$$

where σ_{ys}, σ_{ys}^*, ρ_s and ρ^* refer to compressive yield strength of the cell wall material, compressive yield strength of the

Fig. 4 SEM micrographs of the cell walls of coarse-pored foams at different magnifications. **a** 60×, **b** 1,000× and **c** 5,000×
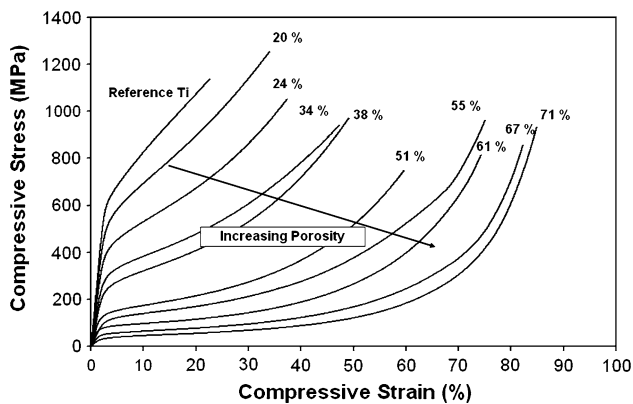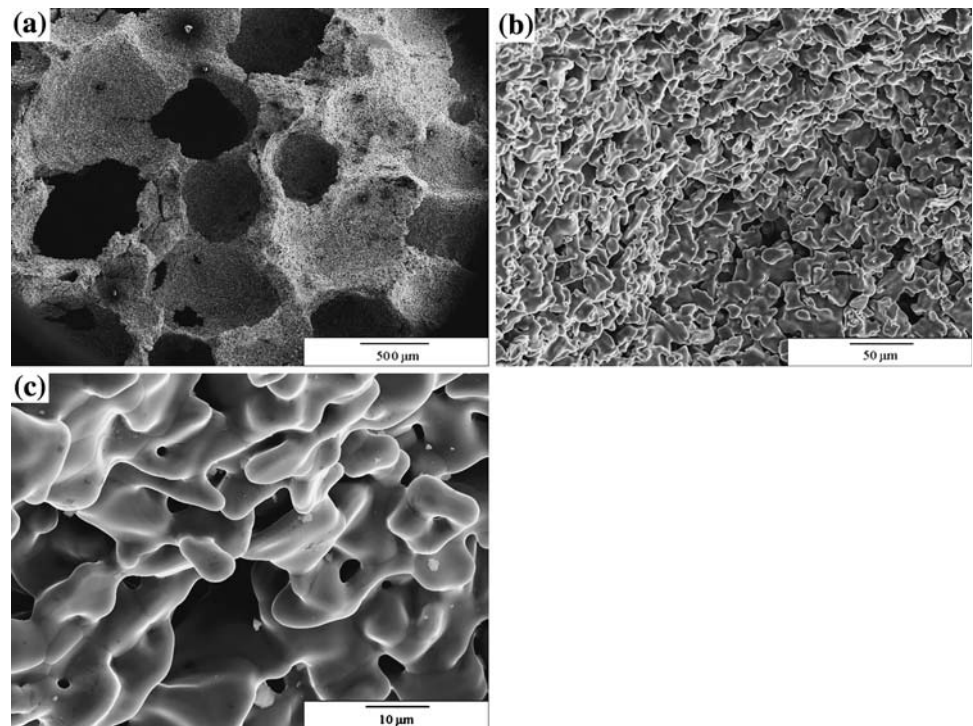

Fig. 5 Compressive stress–compressive strain diagram of fine-pored Ti foams having different levels of porosity. Reference Ti was produced without using space holders

Fig. 6 Relative compressive strength versus relative density plots of the fine- and coarse-pored Ti foams produced

foam, density of the cell material and density of the foam, respectively.

The difference in compressive strengths was not found to be significantly different depending on the pore size (Fig. 6) as seen in the Eqs. 1a and 1b.

The density coefficients in Eqs. 1a and 1b were found to be significantly smaller than those in Imwinkelried's [9] study which is reported as 5.77. This may be explained by the fact that they employed a higher sintering temperature and time than was used in this study leading to the formation of denser pore walls. The major deviation from the Gibson and Ashby's model is that the linear regression lines do not pass through zero. This is not astonishing as
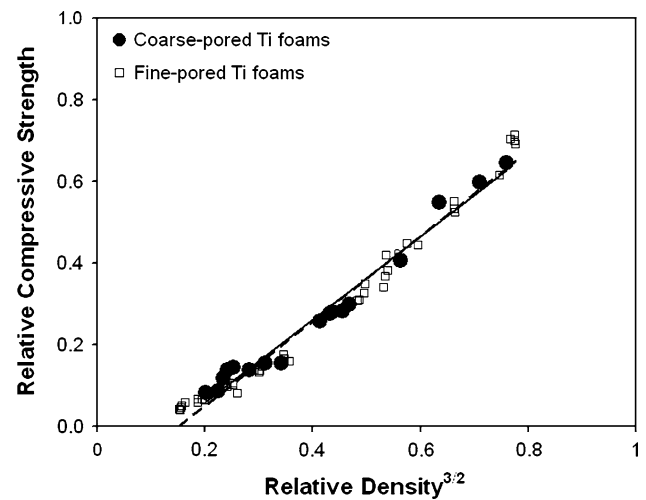
the Ti foam has an irregular pore structure and therefore contains pore walls which do not fully contribute to load bearing [9].

Elastic moduli did not alter when the pore size changed, but a difference in compression behaviour was observed (Fig. 7), in agreement with the results of Bram et al. [10]. At lower strains (the 0.2% offset) Ti foams having coarse pores had slightly higher stress values than those having fine pores, whereas at higher strains the reverse case was observed and the discrepancy in stress values was more pronounced with increasing strain (Fig. 7). Bram et al. [10]
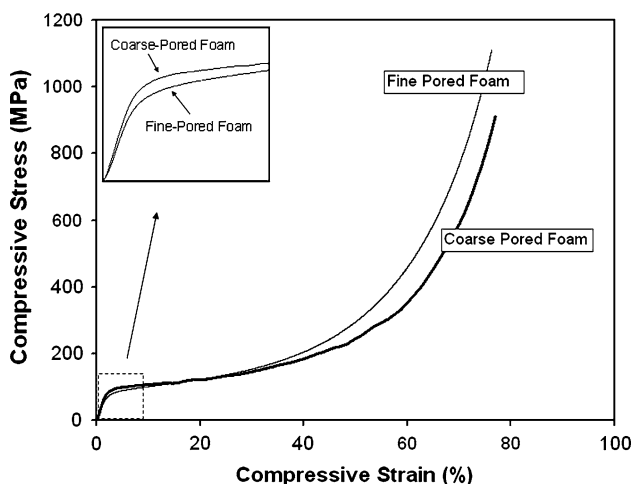
Fig. 7 Compressive stress–compressive strain diagrams of two Ti foams with fine and coarse pores both having 70% porosity

Fig. 9 Plot of relative compressive strength versus the square of relative density of fine-pored Ti foams tested at strain rates of 10^{-3} and 10^{-1} s^{-1}

attributed this behaviour to the faster closure of fine pores in early stages (lower strain regime) of compression.

Effect of strain rate on mechanical properties

A few numbers of mechanical studies on strain-rate sensitivity of bulk Ti are available in the literature. Chichili et al. [11] studied high strain response of Grade 2 and they concluded that the effective flow stress increases with increasing strain rate. Although Silva and Ramesh [12] found that fully dense and porous Ti6Al4V alloys show essentially the same rate-dependence, the literature lacks studies on strain-rate sensitivity of Ti foams. Figures 8 and 9 show the effect of strain rate on relative elastic moduli and compressive strengths of Ti foams, respectively, as a
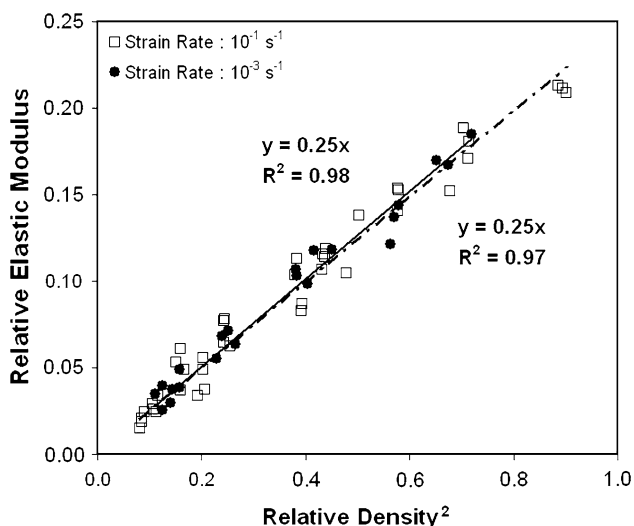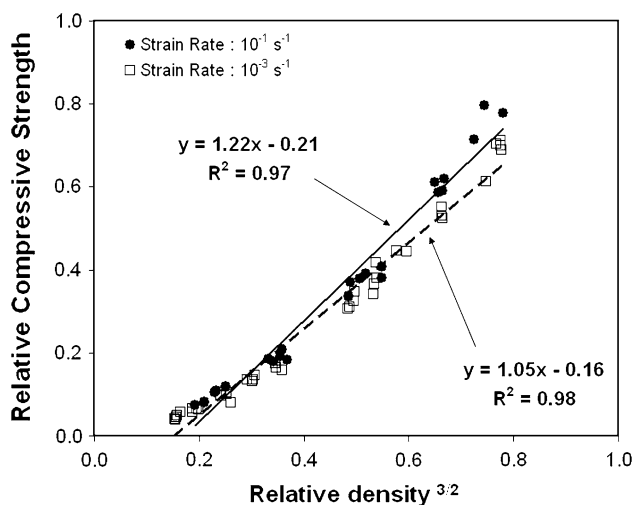
function of relative density. It is apparent that a 100-fold increase in strain rate did not significantly alter the relationship between relative elastic modulus and relative density. However, a slight increase in compressive strength was observed when the strain rate was increased, in accordance with [1]. Preliminary results obtained in this study infer that porous Ti shows a more significant response to higher strain rates (Fig. 10).

Energy absorption

The energy absorption capacity of Ti foams is a topic of discussion which has not been exploited in the literature yet.
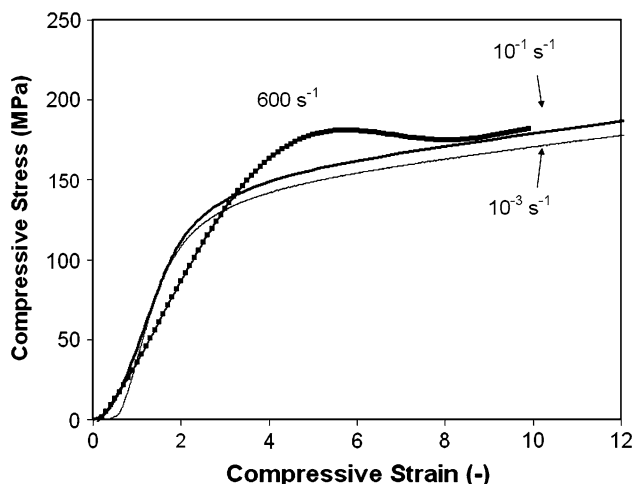

Fig. 8 Plot of relative elastic moduli versus the square of relative density of fine-pored Ti foams tested at strain rates of 10^{-3} and 10^{-1} s^{-1}. An R-squared of 1.0 indicates a perfect fit

Fig. 10 Compressive stress–compressive strain diagram of a Ti foam having 50% fine porosity tested at strain rates of 10^{-3}, 10^{-1} and 600 s^{-1}

The energy absorption capacity is defined as the energy necessary to deform a given specimen to specific strains and is the area under the stress–strain curve up to the densification strain. The energy absorption per unit volume, E_A, is given by Eq. 2 [1].

$$E_A = \int_0^{\varepsilon_{cd}} \sigma \cdot (\varepsilon) \cdot d\varepsilon \qquad (2)$$

where ε_d represents densification strain.

A linear function to determine the densification strain was introduced in [1], which is given in Eq. 3:

$$\varepsilon_d = 1 - \alpha \cdot \left(\frac{\rho}{\rho_s} \right) \qquad (3)$$

where α is a constant that varies between 1.4 and 2.0.

On the other hand, Li et al. [13] defined and distinguished the two important strain values, densification strain and the onset strain of densification (ε_{cd}), in typical stress–strain diagram of cellular solids. They noted that most publications frequently used the densification strain when the onset strain of densification should be used. Onset strain of densification is the critical strain at which the plateau regime is finished, whereas densification strain is defined as the strain at which the cellular material is completely compacted with further compression. Both play important roles in energy absorption design. In this paper, the onset strain of densification was used to characterize the energy absorption behaviour of the produced Ti foams.

However, there exist uncertainties in the determination of the onset strain of densification [13]. It becomes even more complex for Ti foams due to their ambiguous plateau regions. There are many approaches regarding the determination of the onset strain. Some researchers defined the onset strain as the one at which the slope of the tangent is equal to that of the elastic regime [14, 15]. Another approach assumes that the intersection of the tangents to the stress plateau and densification regimes identifies the onset strain of densification [16]. Li et al. [13], in a more recent publication, suggests the use of an energy efficiency equation (Eq. 4). In that approach, the onset strain of densification is defined as the strain at which the slope of the curve in a plot of energy efficiency (η) versus strain (ε) is zero (Eq. 5).

$$\eta(\varepsilon) = \frac{1}{\sigma(\varepsilon)} \cdot \int_0^{\varepsilon} \sigma(\varepsilon) \cdot d\varepsilon \qquad (4)$$

$$\frac{d\eta(\varepsilon)}{d\varepsilon}\Big|_{\varepsilon=\varepsilon_{cd}} = 0 \qquad (5)$$

Based on the experimental data and Eqs. 3 and 4, the onset strain of densification of fine-pored Ti foams having
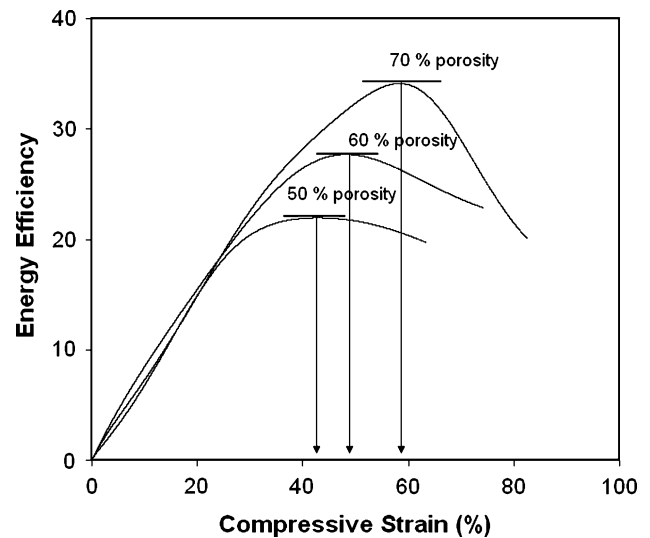

Fig. 11 Energy efficiency–strain curves of three Ti foams having 50, 60 and 70% porosity
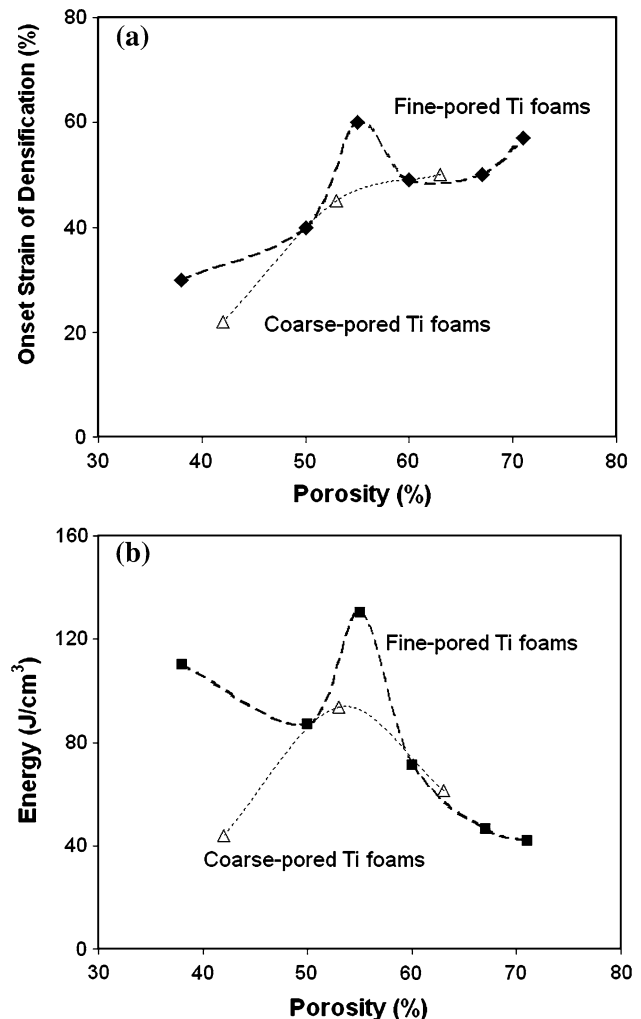

Fig. 12 a Onset strain of densification, b energy absorbed of the fine- and coarse-pored Ti foams

porosities of 50, 60 and 70% were found as 40, 49 and 57%, respectively (Fig. 11). The data of three samples for each porosity level were integrated according to the Eq. 4 and the average of the peak values was taken as the onset strain for each porosity level. The onset strains of densification values determined by the intersection of tangents method were greater than those determined by the efficiency approach, in agreement with the work of Chan and Xie [14]. The energy efficiency approach revealed that there is an optimum porosity level at which onset strain of densification, and accordingly energy absorbed at the onset strain, reach their maxima [15, 17].

The optimum porosity level giving the maximum energy amount absorbed was determined via energy-porosity plots for aluminium and nickel also in [15, 17] and found to be as approximately 70%. In this study, the optimum porosity giving the highest energy absorbed was found as around 55% for both fine- and coarse-pored Ti foams (Fig. 12).

Gibson and Ashby [1] worked out different equations for the three distinct regions of a typical stress–strain diagram for foams. However, when the energy absorbed by the Ti foams at various strains (Fig. 13) is considered, it is proposed that there is a certain trend, fitting to an equation having porosity content and %strain as the independent variables. The trendlines of the curves representing the absorbed energy variation with respect to relative density showed that the energy absorbed per unit volume is proportional to some power of percent strain and relative density.

$$E_A \cong A(\%\varepsilon)^B \left(\frac{\rho^*}{\rho_S}\right)^C \qquad (6)$$

Table 2 Coefficients in Eq. 6 for fine- and coarse-pored Ti foams

Ti foams	A	B	C
Fine-pored	2.4	1.5	2.6
Coarse-pored	2.8	1.4	2.4

where %ε is any strain level. A, B and C are constants which are listed in Table 2 for fine- and coarse-pored foams. Slightly higher exponential constants imply higher energy absorption capability in fine-pored Ti foams especially for higher strains and relative densities.

Conclusions

Elastic moduli did not alter when the pore size changed, but the compressive strength of fine-pored Ti foams was observed to be slightly larger than that of coarse-pored ones.

In the range investigated in this study, strain rate did not significantly affect elastic modulus, but a slight increase in compressive strength was observed when the strain rate was increased from 10^{-3} to 10^{-1} s^{-1}. A more pronounced rise in compressive strength was observed when the strain-rate further increased.

The onset strain of densification of the produced Ti foams was determined via the energy efficiency approach. The energy absorbed per unit volume is affected by the pore size. Fine-pored foams were found to have a higher energy absorption capability. Optimum porosity for
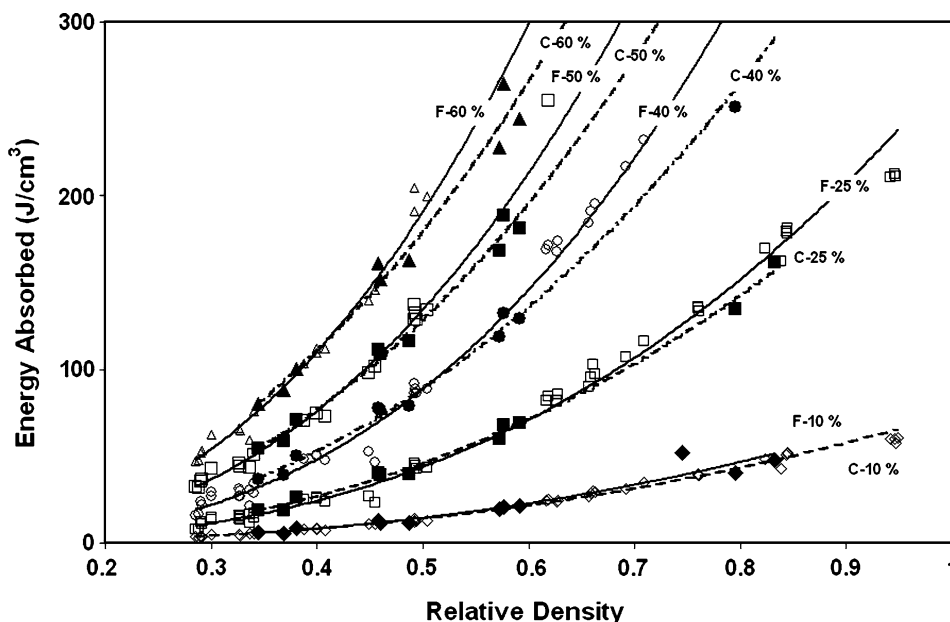

Fig. 13 Energy absorbed versus relative density of fine- (F) and coarse- (C) pored Ti foams at various strains

maximum energy absorption was found to be around 55% for both fine and coarse Ti foams.

When the energy absorbed per unit volume of all the produced Ti foams are plotted as a function of relative density at various strains, it is seen that all the curves can be nicely fitted to an equation of the form:

$$E_A \cong A(\%\varepsilon)^B \left(\frac{\rho}{\rho_S}\right)^C$$

References

1. Gibson LG, Ashby MF (1997) Cellular solids, structures and properties, 2nd edn. Cambridge University Press, Cambridge
2. Banhart J (2002) In: Degischer H-P, Kriszt B (eds) Handbook of cellular metals. Wiley-VCH, Weinheim, p 313
3. Thelen S, Barthelat F, Brinson LC (2004) J Biomed Mater Res 69A:601
4. Salimon A, Brechet Y, Ashby MF, Greer AL (2005) J Mater Sci 40:5793. doi:10.1007/s10853-005-4993-x
5. Balch DK, O'Dawyer JG, Davis GR, Cady CM, Gray GT, Dunand DC (2005) Mater Sci Eng A 391:408
6. Park C, Nutt SR (2002) Mater Sci Eng A 323:358
7. Tuncer N, Arslan G (2007) Effect of processing parameters on compressive behavior of Ti foams. In: MetFoam 2007 conference on porous metals and metallic foams proceedings, Montreal, p 287
8. ASTM designation F67–89 (1994) Standard specification of unalloyed titanium for surgical implants. ASTM, Philadelphia, PA, USA
9. Imwinkelried T (2007) J Biomed Mater Res A 81:964
10. Bram M, Schiefer H, Bogdanski D, Köller M, Buchkremer HP, Stöver D (2006) Met Powder Rep 61(2):26
11. Chichili DR, Ramesh KT, Hemker KJ (1998) Acta Mater 46:1025
12. Silva MG, Ramesh KT (1997) Mater Sci Eng A232:11
13. Li QM, Magkiriadis I, Harrigan JJ (2006) J Cell Plast 42:371
14. Chan KC, Xie LS (2003) Scr Mater 48:1147
15. Tzeng S-C, Ma W-P (2007) Int J Adv Manuf Technol 32:473
16. Paul A, Ramamurty U (2000) Mater Sci Eng A 281:1
17. Firstov SA, Podrezov YN, Lugovoi NI, Slyunyaev VN, Verbilo DG (2000) Powder Metall Met Ceram 39:407